Mem. S.A.It. Vol. 91, 249

Memorie della

Non-linear simulations of the Tayler instability

A. Bonanno[1], G. Guerrero[2], and F. Del Sordo[1]

[1] Istituto Nazionale di Astrofisica – Osservatorio Astrofisico di Catania, Via S.Sofia 78, 95123 Catania, Italy, e-mail: alfio.bonanno@inaf.it
[2] UFMG – Departamento de Fisica, Rua Professor Giorgio Schereiber 90, 31270-901 Belo Horizonte, Brazil

Abstract. The evolution of toroidal field instability is essential to understand the topology of the magnetic fields observed in early-type stars, or in the isothermal core of the red giants. We study the non-linear evolution of the instability of a predominant toroidal field stored in a stably stratified stellar interior in spherical symmetry. In particular we followed the non-linear phase in order to understand the role of stable stratification in suppressing the instability. We use the MHD equations as implemented in the anelastic approximation in the EULAG code and perform a series of high-resolution numerical simulations of the instability exploring a large parameter space. We show that beyond a critical value gravity strongly suppress the instability, in agreement with the linear analysis. the intensity of the initial field also plays a crucial role, as weaker fields show much lower growth rates. Moreover, the fastest growing modes have a very large characteristic radial scale, at variance with recent claims from the linear analysis. Our results illustrate that the anelastic approximation can efficiently describe the evolution of toroidal field instability in realistic stellar interior. The suppression of the instability as consequence of stratification can likely play a role to explain the magnetic desert in Ap/Bp stars, since weak fields are only marginally unstable in the case of strong gravity.

1. Introduction

The EULAG code was originally designed to model atmospheric (multi-scale) flows and is widely known for its success in that area (Prusa et al. 2008). Recently an MHD extension of the code allows to perform simulations of solar and stellar dynamos (Smolarkiewicz & Charbonneau 2013). The versatility of EULAG relies on its generalized curvilinear coordinates formulation with the non-oscilatory forward-in-time (NFT) differencing scheme based on MPDATA (Smolarkiewicz et al. 2001) and a robust elliptic solver (Smolarkiewicz et al. 1997).

The MHD equations are solved without considering the dissipative terms. Therefore, the only dissipation is of numerical origin and is minimized by the MPDATA scheme. This allows to maximize the Reynolds and the magnetic Reynolds numbers of the simulations for any given resolution producing a well resolved turbulence. Furthermore, the numerical dissipation introduced by the method has been identified as the contribution of the non-resolved scales normally implemented in turbulence modeling. For this reason the method corresponds to an implicit large eddy class of models (Margolin & Rider 2002).

The code has been used for simulations of the Sun and solar-like stars, as well as for young stars with a fully convective interior or a small radiative zone (Ghizaru et al. 2010;

Table 1. Results of simulations with three values of gravity (g=50, 100, 150). The columns indicate the gravity g_0, the initial magnetic field B_0, The Brunt-Vaisala frequency ω_{BV}, the Alfven frequency ω_A, the bottom to top density contrast ρ_b/ρ_t, the parameter δ, the ratio of poloidal to toroidal magnetic field at the end of the linear phase of the instability B_p/B_t, and the growth rate Γ. For each value of g we varied the magnetic field in the range $1 - 10^{-2}$ T. The growth rates marked with * are compatible with zero, as the relative simulations have never reached the linear growth phase. These values were therefore calculated when the magnetic fields were still noisy. and consequently they are not reliable. We decided to include them anyways for completeness.

Model	g_0	B_0	$\omega_{BV} \cdot 10^{-4}$	$\omega_A \cdot 10^{-9}$	ρ_b/ρ_t	δ	B_p/B_t	Γ
TiB50a	50	0.01	0.68	2.5	1.18	27265.64	0.0	0.17
TiB50b	50	0.05	0.68	12.53	1.18	5453.16	0.00	0.21
TiB50c	50	0.10	0.68	25.06	1.18	2726.57	0.01	0.24
TiB50d	50	0.50	0.68	125.32	1.18	545.31	0.06	0.57
TiB50e	50	0.65	0.68	162.91	1.18	419.47	0.08	0.81
TiB50f	50	1.00	0.68	250.62	1.18	272.68	0.13	0.79
TiB100a	100	0.01	1.37	2.60	1.40	52588.24	0.00	0.01 *
TiB100b	100	0.05	1.37	12.99	1.40	10517.69	0.00	0.04
TiB100c	100	0.10	1.37	25.99	1.40	5258.82	0.00	0.10
TiB100d	100	0.50	1.37	129.96	1.40	1051.72	0.06	0.34
TiB100e	100	0.65	1.37	168.95	1.40	809.00	0.09	0.37
TiB100f	100	1.00	1.37	259.91	1.40	525.88	0.08	0.56
TiB150a	150	0.01	2.05	2.70	1.66	75871.90	0.00	0.80*
TiB150b	150	0.05	2.05	13.51	1.66	15174.38	0.00	0.26*
TiB150c	150	0.1	2.05	27.02	1.66	7587.19	0.00	0.04
TiB150d	150	0.50	2.05	135.12	1.66	1517.44	0.01	0.28
TiB150e	150	0.65	2.05	175.65	1.66	1167.28	0.07	0.28
TiB150f	150	1.00	2.05	270.24	1.66	758.72	0.10	0.34

Guerrero et al. 2016; Zaire et al. 2017). Two mayor breakthroughs have been achieved with the EULAG-MHD code (Ghizaru et al. 2010). The first one is the natural development of the shear layer called tachocline, at the interface between radiative and convection zones. This occurs because of the lower value of the numerical viscosity which prevents the angular momentum to be transported towards the radiative zone. The second is the attainment of magnetic field reversals, and therefore of magnetic cyclic activity. By capturing the contribution of the non-resolved small scales via the MPDATA scheme, the magnetic field sources get appropriate values to result in periodic behavior. These features are highly appealing for the goals described above.

2. The setup and results

We solve the anelastic MHD equations in the following form:

$$\boldsymbol{\nabla} \cdot (\rho_{\rm ad} \boldsymbol{u}) = 0, \tag{1}$$

$$\frac{D\boldsymbol{u}}{Dt} = -\boldsymbol{\nabla}\left(\frac{p'}{\rho_{\rm ad}}\right) + \boldsymbol{g}\frac{\Theta'}{\Theta_{\rm ad}} + \frac{1}{\mu_0 \rho_{\rm ad}}(\boldsymbol{B}\cdot\nabla)\boldsymbol{B}\,, \tag{2}$$

$$\frac{D\Theta'}{Dt} = -\boldsymbol{u}\cdot\boldsymbol{\nabla}\Theta_{\rm amb} - \frac{\Theta'}{\tau}\,, \tag{3}$$

$$\frac{D\boldsymbol{B}}{Dt} = (\boldsymbol{B}\cdot\nabla)\boldsymbol{u} - \boldsymbol{B}(\nabla\cdot\boldsymbol{u})\,, \tag{4}$$

where $D/Dt = \partial/\partial t + \boldsymbol{u}\cdot\boldsymbol{\nabla}$ is the total time derivative, $\boldsymbol{u}$ is the velocity field, p' is a pressure perturbation variable that accounts for

both the gas and magnetic pressure, and $\boldsymbol{B}$ is the magnetic field. The energy equation is written in terms of perturbations of the potential temperature, Θ'. It accounts for fluctuations of the temperature from an adiabatic towards an ambient state, $\Theta_{\rm amb}$. The latter is chosen to be roughly isothermal $\rho_{\rm ad}$ and $\Theta_{\rm ad}$ are the density and potential temperature of the reference isentropic state (i.e., $\Theta_{\rm ad}$ = const) in hydrostatic equilibrium; $g = \frac{g_0}{(r/r_b)^2}\hat{\boldsymbol{e}}_r$ is the gravity acceleration, with g_0 its value at the bottom of the domain where $r = r_b$; and μ_0 is the magnetic permeability of the vacuum. The potential temperature, Θ, is related to the specific entropy: $s = c_p \ln\Theta$ + const.

We consider a spherical shell with $0 \leq \varphi \leq 2\pi$, $0 \leq \theta \leq \pi$ and a radial extent from $r_b = 0.4R_\odot$ to $r_t = 0.96R_\odot$. The boundary conditions are defined as follows: for the velocity field we use impermeable, stress-free conditions at the top and bottom surfaces of the shell; for the magnetic field we consider a perfect conductor at both boundaries. Finally, for the thermal boundary condition we consider zero radial flux of potential temperature. The simulations mesh in most of the simulations has $126 \times 42 \times 72$ grid points in the φ, θ and r directions, respectively. The constant time-step of the simulations is $\Delta t = 1800$ s. For the high resolution simulations we double the number of grid points on each direction and decrease the time-step to $\Delta t = 400$ s.

The reference and ambient states are computed by solving the hydrostatic equilibrium equations for a polytropic atmosphere,

$$\frac{\partial T_{\rm i}}{\partial r} = -\frac{g}{R_g(m_{\rm i}+1)}\,, \tag{5}$$

$$\frac{\partial \rho_{\rm i}}{\partial r} = = -\frac{\rho_{\rm i}}{T_{\rm i}}\left(\frac{g}{R_g} - \frac{\partial T_{\rm i}}{\partial r}\right)\,, \tag{6}$$

Density and temperature are related to the gas pressure through the equation of state for a perfect gas, $p_{\rm i} = R_g\rho_{\rm i}T_{\rm i}$. The initial values to solve this equations are $\rho_0 = 37$ km $\cdot$ m^{-3} and $T_0 = 3.5 \times 10^6$ K. Different values of g_0 allow to obtain different degrees of stratification.Finally, adiabatic and isothermal atmospheres are obtained with the polytropic indexes $m_{\rm ad} = 1.5$ and $m_{\rm amb} = 10^3$, respectively.

The simulations start with a purely toroidal magnetic field, i.e.,

$$\begin{aligned} B_{r0} &= 0 \\ B_{\theta 0} &= 0 \\ B_{\varphi 0} &= 2B_0 \sin\theta\cos\theta f(r)\,, \end{aligned} \tag{7}$$

where

$$f(r) = \exp\left(-(r-r_0)^2/\omega^2\right), \tag{8}$$

where $r_0 = 0.68R_\odot$, $\omega = 0.5R_\odot$, and B_0 is the maximum amplitude of the initial magnetic field which is a free parameter in the simulations.

We define $\tilde{\delta}^2 = \tilde{\omega}_{BV}^2/\tilde{\omega}_A^2$, with

$$\tilde{\omega}_{BV}^2 = \langle\frac{g}{\Theta_{\rm amb}}\frac{\partial\Theta_{\rm amb}}{\partial r}\rangle_r,\quad \tilde{\omega}_A^2 = \langle\frac{B_{\varphi 0}^2}{\mu_0\rho_{\rm amb}\omega^2}\rangle_{r,\theta}. \tag{9}$$

Here, the angular brackets represent averages in the radial direction for the Brunt-Vaisäla and in radius and latitude (over one hemisphere) for the Alfven frequency. The values of $\tilde{\omega}_{BV}$, $\tilde{\omega}_A$ and $\tilde{\delta}$ are presented in the table below, while a full evolution of the instability is presented in the figure.

By construction our initial state is Tayler unstable. Therefore, it is expected that the instability develops after a few characteristic Alfven travel times. This occurs for the models with strongest initial magnetic fields. The simulations with weaker fields ($B_0 \leq 0.5$ T) reach magnetohydrostatic equilibrium after about one Alfven travel times. Therefore, we impose a white noise perturbation and continue the simulations for, at least, 20 Alfven travel times.

3. Conclusions

We presented numerical simulations of the evolution of toroidal magnetic fields in a stably stratified environment. Our approach was aimed at studying the evolution of an unstable magnetic field configuration in order to assess the role played by gravity in the occurrence of the instability. First of all, we presented the first

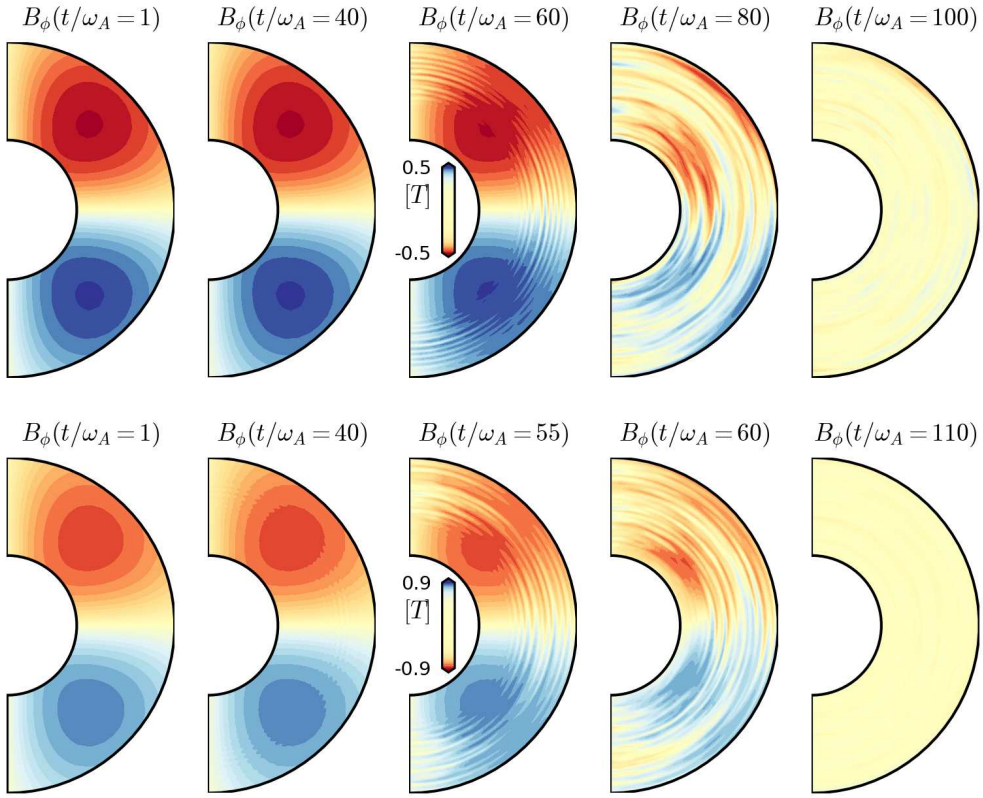

Fig. 1. Contourplots of the azimuthal component of the magnetic field at different times for two models with g=100. TiB100d (top), with B_0 = 0.5T, and TiB100e (bottom), with B_0 = 0.65T.

simulations of Tayler instability in the anelastic approximation. We showed how our numerical setup is able to reproduce the main features of this instability. Second, we illustrated how gravity plays a role in the stabilization of the field. The stronger the gravity, the more stable the field. In the case of very strong magnetic field (B=1 T) in the initial configuration, we observe how for small gravity the system immediately undergoes the instability. The contrary happens for strong gravity: although the gravity cannot completely suppress the instability, which occurs on times of the order of 100 Alfven travel times, the instability presents a growth rate much weaker. In the case of weaker initial magnetic field we observe a clear suppression of the instability. Our simulations do not go unstable for g=100 and B=0.01 T on timescales of about 20 Alfven travel times. Nonetheless we cannot exclude the instability will occur later on, after more than hundred t_A.

In the future we plan to extend this analysis including the effect of rotation and of the presence of another field.

3.1. CINECA

The role of CINECA was essential in provinding our group the necessary computational power to develop this study. A paper has been almost submitted on A&A and we are currently styding the possibility of applying for larger projects in order to study the evolution of a typical A star from MS to the Red Giant phase. I think that the allocation of CINECA resources

via the INAF agreement works rather well for this type of research.

Acknowledgements. We acknowledge the computing centre of Cineca and INAF, under the coordination of the "Accordo Quadro MoU per lo svolgimento di attività congiunta di ricerca Nuove frontiere in Astrofisica: HPC e Data Exploration di nuova generazione", for the availability of computing resources and support.

References

Ghizaru, M., et al. 2010, ApJ, 715, L133

Guerrero, G., et al. 2016, ApJ, 819, 104

Margolin, L. G. & Rider, W. J. 2002, Int. J. Numer. Meth. Fluids, 39, 821

Prusa, J. M., et al. 2008, Computers & Fluids, 37, 1193

Smolarkiewicz, P. K., et al. 1997, Mon. Weather Rev., 125, 647

Smolarkiewicz, P. K., et al. 2001, J. Atmos. Sci., 58, 349

Smolarkiewicz, P. K. & Charbonneau, P. 2013, J. Comput. Phys., 236, 608

Zaire, B., et al. 2017, IAU Symposium, 328, 30